

# ENHANCEMENT OF LASCO C1, C2, AND C3 CORONAGRAPH IMAGES

NRL Grant N00014-97-1-GO23

Annual Report

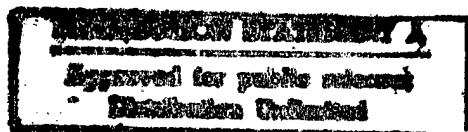
For the Period 1 February 1997 through 31 January 1998

Principal Investigator  
Dr. Margarita Karovska

July 1998

Prepared for:

Department of the Navy  
Naval Research Laboratory  
Washington, D.C. 20375-5326



19980915 109

Smithsonian Institution  
Astrophysical Observatory  
Cambridge, Massachusetts 02138

The Smithsonian Astrophysical Observatory  
is a member of the  
Harvard-Smithsonian Center for Astrophysics

The NRL Scientific Officer for this grant is Richard Rubin, Naval Research Laboratory,  
CODE 7605.10, 4555 Overlook Avenue S.W., Washington, D.C. 20375-5326.



SMITHSONIAN ASTROPHYSICAL OBSERVATORY  
60 Garden Street, Cambridge, MA 02138

(617) 495-7000

10 September 1998

Mr. Richard Rubin  
Program Officer  
Naval Research Laboratory  
Code 7605.10  
4555 Overlook Avenue, SW  
Washington, DC 20375-5326


Subject: Annual Report

Reference: Grant N00014-97-1-G023

Dear Mr. Rubin:

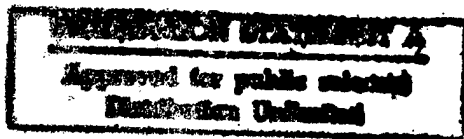
Transmitted herewith is one (1) copy of the subject report for the period 1 February 1997 through 31 January 1998, in accordance with the provisions of the above referenced grant.

Very truly yours,

*for*   
John G. Harris  
Manager,  
Contracts, Grants & Property Management

JGH/rn  
Enclosure

cc: Director, Naval Research Laboratory, Code 5227, 4555 Overlook Avenue, SW,  
Washington, DC 20375-5326, w/encl.  
Defense Technical Information Center, 8725 John J. Kingman Road, Suite  
0944, Ft. Belvoir, Virginia 22060-6218, w/encl.



# Enhancement of LASCO C1, C2 and C3 Coronagraph Images

Margarita Karovska and Brian Wood

Harvard-Smithsonian Center for Astrophysics, Cambridge, MA 02138

## 1. Introduction

The Large Angle Spectrometric Coronagraph (LASCO) onboard SOHO provided unprecedented views of the solar corona since January 1996. This instrument contains three individual coronagraphs C1, C2, and C3, described in detail in Brueckner et al (1995). The C1 coronagraph acquires high resolution images (11" and higher) of the lower corona from 1.1  $R_{\odot}$  to 3.0  $R_{\odot}$ , thereby providing a close link to the disk observations of other instruments in the SOHO complement. The C2 and C3 images have lower resolution (23" and about 2' respectively), however they provide a unique view of the extended corona up to 32  $R_{\odot}$ . LASCO multiwavelength images contain many complex structures at different spatial scales, and the brightness difference between various features is often very high.

During the past year we carried out a study of the morphology and dynamical evolution of structures in the solar corona. This included coronal mass ejections, and polar jets as observed by LASCO (and EIT). We applied image enhancement techniques to LASCO images to enhance the small scale structures and/or the low contrast structures in CMEs and in the polar coronal regions. In the following, we summarize the results of this studies.

## 2. Coronal Mass Ejections and Testing of a Flux Rope Model

We studied the morphology of a large number of CMEs using image enhancement techniques to extract the low contrast structures. As an example, we describe here our analysis of two CMEs (from 1997 April 30 and 1997 February 23), and the results of our testing of the viability of an MHD model of expanding flux rope developed by Chen et al. (1997).

Like the CME from 1997 April 13 used by Chen et al. to carry out the initial tests of their model, these two CMEs had a particularly well-defined structure that maintained its integrity throughout the course of the observations. These two CMEs are clearly detected in all three LASCO coronagraphs (C1, C2, and C3), and in EIT images as well, in contrast to the April 13 CME which was only seen in C2 and C3. Thus, the April 30 and February 23 CMEs allow for a more detailed comparison with the predictions of the flux rope model.

Several C2 images of the April 30 and February 23 CMEs are shown in Figures 1 and 2, respectively. These images are shown both after the background is subtracted using an average-differencing technique (upper panels) and after edge-enhancement (lower panels). The CME on February 23 is accompanied by a dramatic prominence eruption and a significant GOES X-ray flare, while the April 30 CME is accompanied by no apparent prominence eruption and only a weak X-ray flare. In the C2 and C3 fields of view, both CMEs show the same basic structure as the April 13 CME — a circular rim surrounding a relatively dark cavity containing bright material near the trailing edge.

In Figures 1–2, the locations of the leading edge (plus signs), trailing edge (X’s), and sides (asterisks) of the CMEs are indicated. These measurements are used to compute the centroids of the CMEs, which are also shown in the figures (circles). In the top panels of Figures 3 and 4, height-vs.-time plots are displayed for the leading edge, centroid, and trailing edge of the two CMEs.

By taking the first and second derivatives of the height curves, we derived empirical velocity and acceleration curves. We experimented with different techniques for doing this. In Figures 3–4, we derived the velocity and acceleration curves by first fitting polynomials to the height data and then analytically computing the derivatives. Simple second order polynomials are sufficient to fit the centroid and trailing edge curves. Much higher order polynomials are required to fit the leading edge curves, so rather than fitting a single polynomial to the data, we broke the curves into two pieces and fitted two separate polynomials to them. For the April 30 data, second order polynomials were sufficient to fit both pieces, while for the February 23 data a fourth order polynomial was used for the first piece and a second order polynomial for the second.

The resulting velocity and acceleration curves are plotted in the bottom two panels of Figures 3–4, along with  $1\sigma$  uncertainties estimated using Monte Carlo techniques. The acceleration of both CMEs occurs below about  $4 R_{\odot}$ . The very fast leading edge of the February 23 CME reaches speeds of about  $900 \text{ km s}^{-1}$  before leveling off in the the C2 field of view, while the relatively slow April 30 CME only attains speeds of about  $300 \text{ km s}^{-1}$ .

We compared the measured kinematic properties of the two CMEs with the predictions of the erupting flux rope model discussed by Chen et al. (1997) and Chen (1996). Both of our CMEs have well-defined circular rims which can be interpreted as marking the outline of the apex of the flux rope as viewed from the side, meaning that the flux rope is assumed to have an east-west orientation.

In the model, the initially stable flux rope is set in motion by an increase in the poloidal component of the flux rope’s magnetic field, which is helical in the rope’s interior. The C2 observations of the April 30 CME show helical lines below the rim of the CME (see Fig. 1), which suggests the possible presence of a helical magnetic field such as that assumed in the model. The magnetic flux injection profile  $d\Phi_p/dt$  is the primary free parameter that we use to match the dynamic characteristics of individual CMEs.

Our best fits to the observations are shown in Figures 5 and 6. The top and bottom panels show the measured height and velocity curves from Figures 3–4, along with the flux rope model results. We define an observable aspect ratio,  $\Lambda(t) \equiv R_c(t)/D(t)$ , where  $R_c(t)$  is the heliocentric height of the centroid and  $D(t)$  is the width of the observed circular rim. In the middle panels of Figures 5–6, the observed and model values of  $\Lambda$  are plotted for the CMEs. Also shown in the middle panels are the normalized injection profiles ( $d\Phi_p/dt$ ) used in the flux rope calculations.

Although the theoretical curves in Figures 5 and 6 are not perfect fits to the data, they are close enough to support the claim that the flux rope model has captured the essential physics of the CME. Thus, we have demonstrated that the flux rope model is capable of matching the dynamics of CMEs at early times as well as late times, and is also capable of modeling CMEs with very different velocities and accompanying phenomena.

### 3. Study of Polar Region Coronal Structures

We studied the dynamical evolution of structures in the polar region using a sequence of LASCO/C2 images of the north polar region taken on 1997 March 22 which lasted for about 41 hours. The average time between the 200 images taken during the sequence was 12.2 minutes. Near the end of the sequence, a series of three compact jets of material were ejected from a point near the north pole. In order to study these jets further, we focused our attention on a thin sector centered on the axis of the jets. We partitioned the sector into 72 segments and then measured intensities along the axis of the sector by summing the pixels within these segments. In Figure 7, we display the evolution of these intensity tracings with time. The first and by far the brightest jet is noticeable as a nearly vertical bright streak at  $t = 32$  hr with a positive slope. The other two jets, which are significantly dimmer, follow shortly after the first jet at  $t = 35$  hr and  $t = 37$  hr.

For each intensity tracing where the jet is fully visible, we have fitted a Gaussian to the intensity profile to estimate where the centroid is located.

Both the centroid and leading edge curves show a decreasing slope with time, indicating a deceleration. This behavior is different from that of coronal mass ejections, which generally show continuous acceleration below  $3-4 R_{\odot}$ . The simplest possible interpretation for the deceleration seen for the polar jets is that it is due to gravity. In order to test this interpretation, we fitted the centroid data points with a ballistic trajectory curve and estimated the initial ejection velocity of  $580 \text{ km s}^{-1}$ . This velocity is slightly below the Sun's escape velocity of  $619 \text{ km s}^{-1}$ , suggesting that in the absence of other forces the jet material will fall back toward the Sun.

Movies of the 200 polar images revealed the existence of a bright radial front of enhanced intensity in the northeast quadrant which advances slowly northward while remaining oriented in a radial direction. We believe this is a bright streamer that becomes superimposed onto the Sun's polar region after rotating into the foreground from near the northeast limb. The existence of this foreground material is potentially a serious complication for studies of polar plumes because it is not easy to separate the intensities of the bright plumes from those of the foreground streamer material.

In order to search for other examples of these "brightness fronts", we made a three month-long movie of C2 images, running from 1997 February 1 to 1997 April 30, using data obtained for LASCO's standard solar monitoring program. In reality, only about 1 of 5 available images was used in order to save both time and hard disk space. We detected several fronts in this movie, most in the north polar region and most advancing from east to west. (The few seen advancing eastward would presumably be streamers rotating from the west limb to behind the Sun, and therefore in the background of the polar regions.) A few of the fronts could be tracked for more than 10 days. We measured the position angles of these fronts as they moved from one limb to the other, and Figure 8 shows a plot of position angle versus time for one of the fronts. The other fronts show similar behavior. The shape of the curve is consistent with that of a partial sine wave, as expected if these fronts are simply rotating streamers. We have fitted a sine wave to the data points, and the period of the fitted wave is 22 days. This is roughly equal to the solar rotation period, which is also consistent with these fronts simply being due to streamer belt material rotating into the foreground.

#### 4. Future Plans

We plan to continue our study of the kinematic properties of CMEs and further test and improve the expanding flux rope model of CMEs by Chen et al. (1997). For this project we have compiled an extended sample of CMEs that were observed by both LASCO and EIT. Our original sample used for testing the expanding flux rope model contained only few CMEs. In order to study the dynamics of CMEs at early stages in their development, we are particularly interested in looking for CMEs that were observed by both the LASCO C1 coronagraph and the Mark III coronagraph on Mauna Loa, which have similar fields of view. We hope that the combined data from both instruments will greatly improve the temporal coverage over LASCO C1 data alone. We will continue to use image processing techniques to enhance low contrast structures in the Solar Corona.

We are currently studying three jets from 1997 March 24 LASCO observations when the C2 field of view was limited to the north polar region and C2 was imaging with a higher than nominal cadance. Our goal is to quantify this kinematic behavior and to compare it to the properties of polar jets from a larger sample, and with the CME kinematics.

#### REFERENCES

- Chen, J. 1996, J. Geophys. Res., 101, 27499  
Chen, J., et al. 1997, ApJ, 490, L191  
Wang, Y.-M., et al. 1998, preprint.

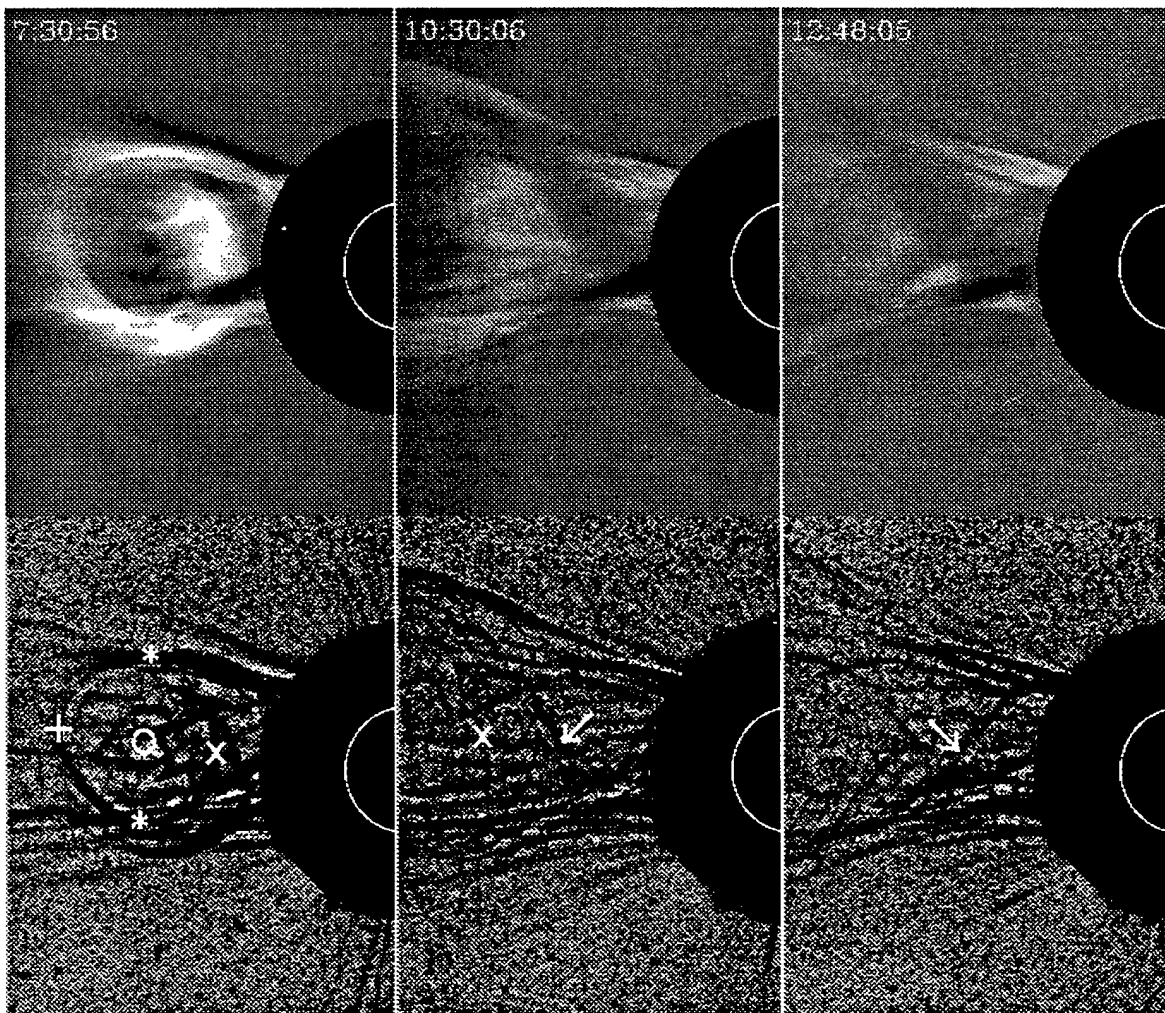


Fig. 1.— Average-differenced and edge-enhanced versions of three LASCO C2 images of the April 30 CME. The locations of the leading edge (plus sign), trailing edge (X's), sides (asterisks), and centroid (circle) of the bright circular rim structure of the CME are indicated. Helical lines are seen below the rim which possibly trace the magnetic field. Two of these lines are identified with arrows.

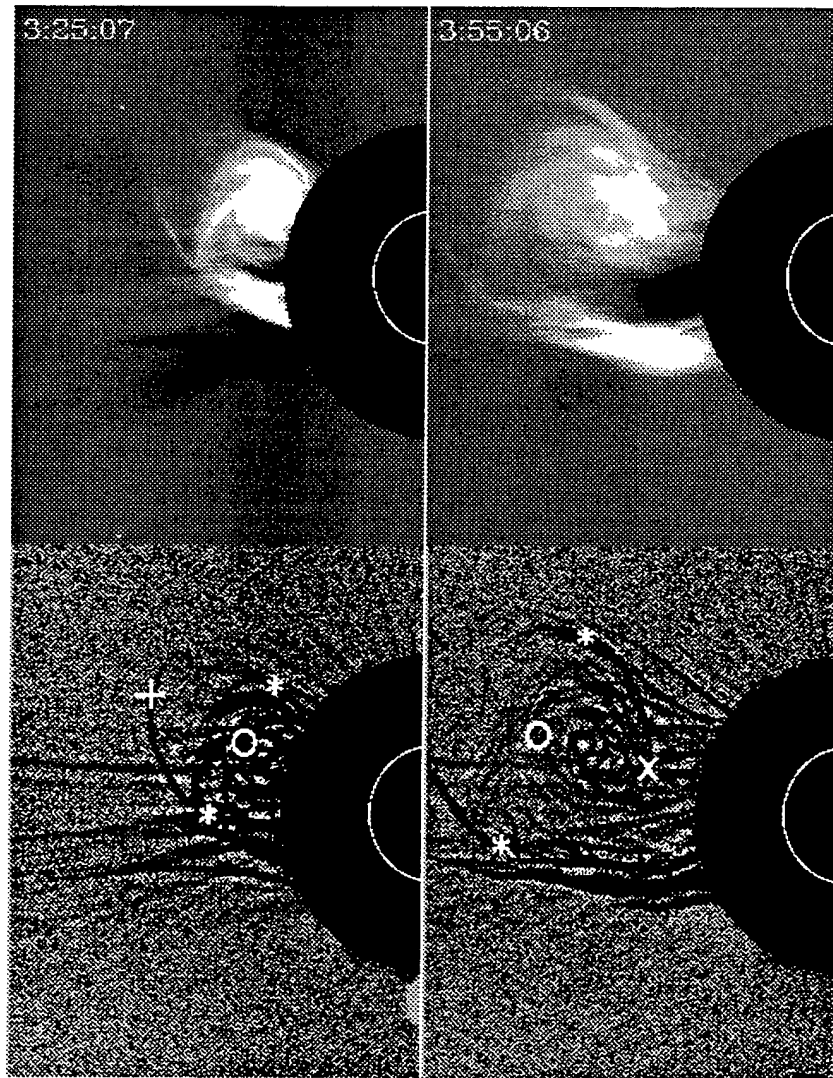


Fig. 2.— Average-differenced and edge-enhanced versions of three LASCO C2 images of the February 23 CME. The locations of the leading edge (plus sign), trailing edge (X), sides (asterisks), and centroid (circles) of the bright circular rim structure of the CME are indicated.



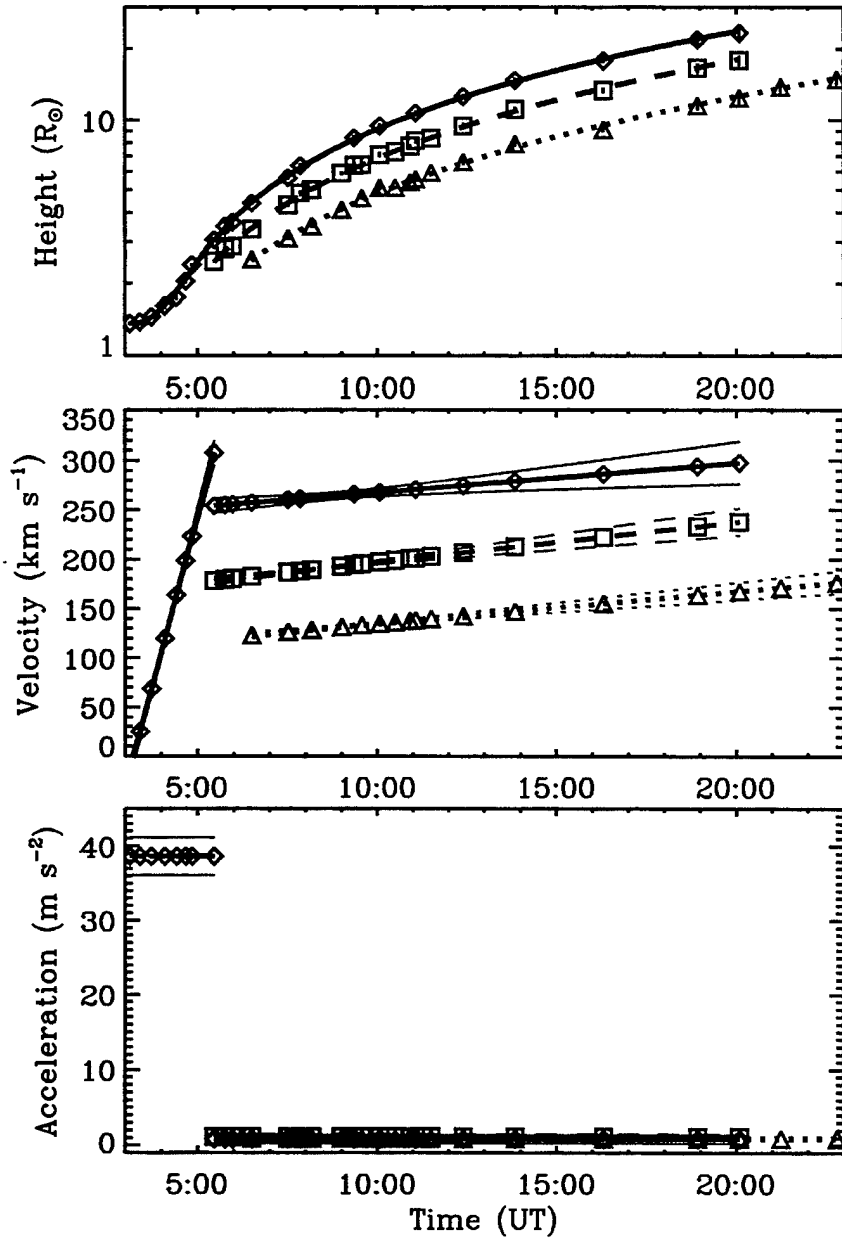


Fig. 3.— Height-, velocity-, and acceleration-vs.-time curves for the leading edge (diamonds, solid lines), centroid (squares, dashed lines), and trailing edge (triangles, dotted lines) of the April 30 CME. The height measurements were fitted with second order polynomials, two separate ones in the case of the leading edge. The velocity and acceleration curves were derived from these fits (thick lines). The thin lines are  $1\sigma$  uncertainties estimated using Monte Carlo techniques.

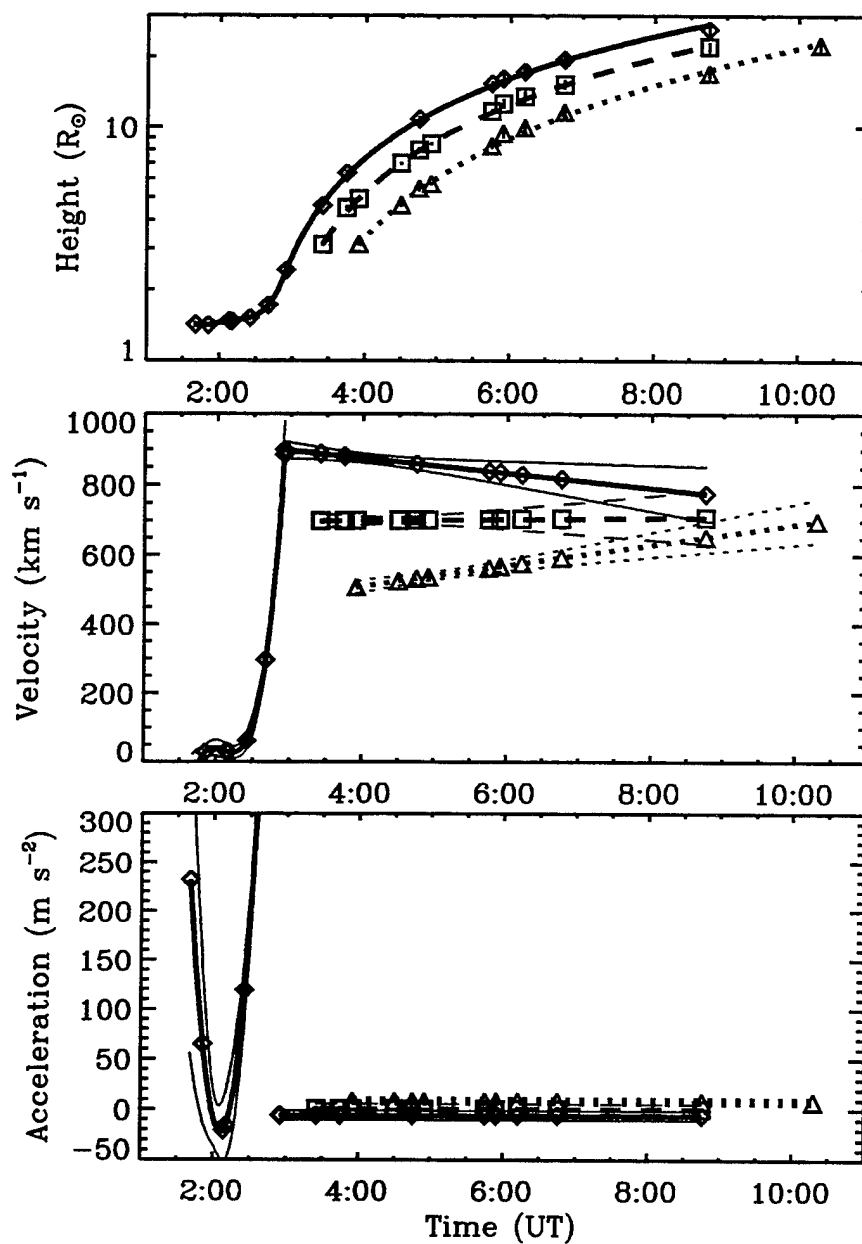


Fig. 4.— Same as Fig. 3, but for the February 23 CME. The fit to the leading edge is a combination of a fourth order polynomial and a second order polynomial rather than the two second order polynomials used for the April 30 CME.

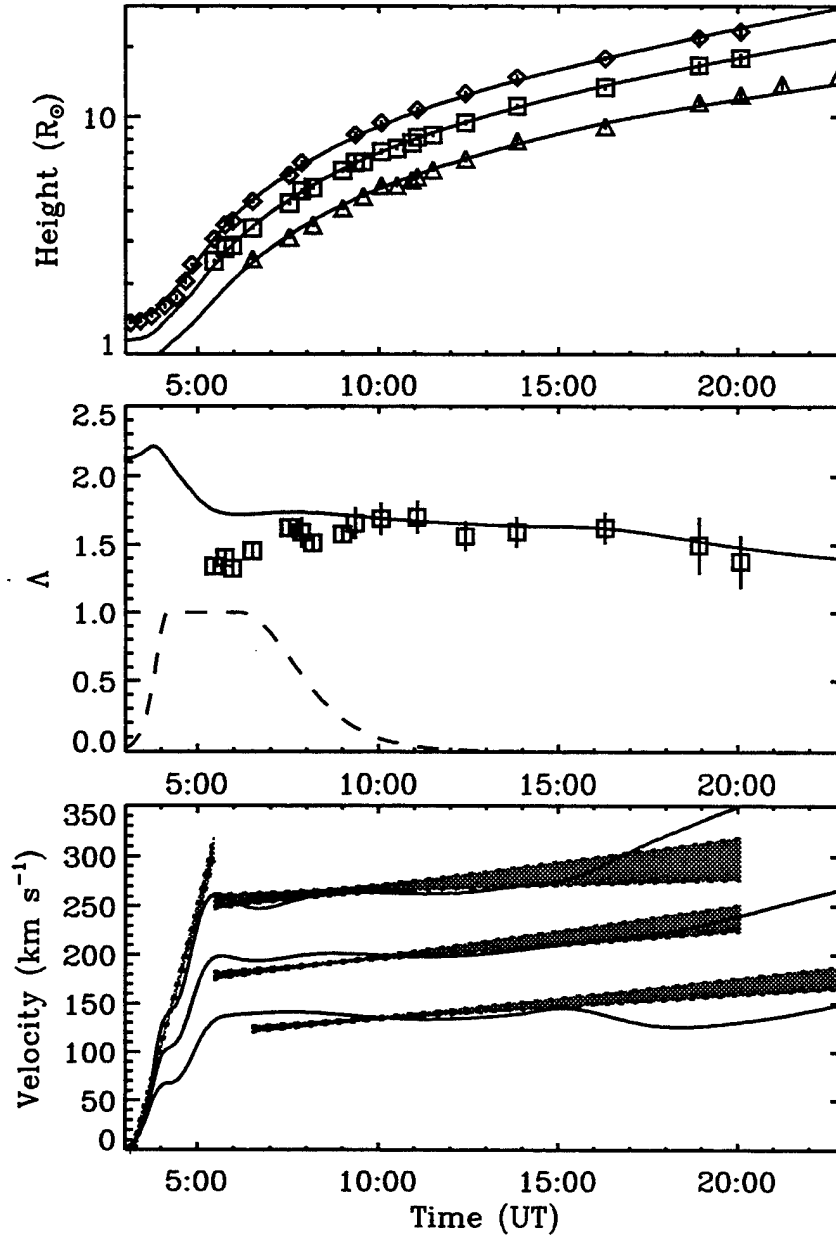


Fig. 5.— In the top panel, the height measurements for the leading edge (diamonds), centroid (boxes), and trailing edge (triangles) of the April 30 CME are plotted; and in the bottom panel the velocity measurements from Fig. 3 are reproduced (shaded regions). These measurements are compared with the theoretical predictions of an expanding flux rope model (solid lines). In the middle panel, both observed and model values for the aspect ratio  $\Lambda$  are plotted. Also shown is a normalized flux injection profile used in the flux rope model (dashed line).

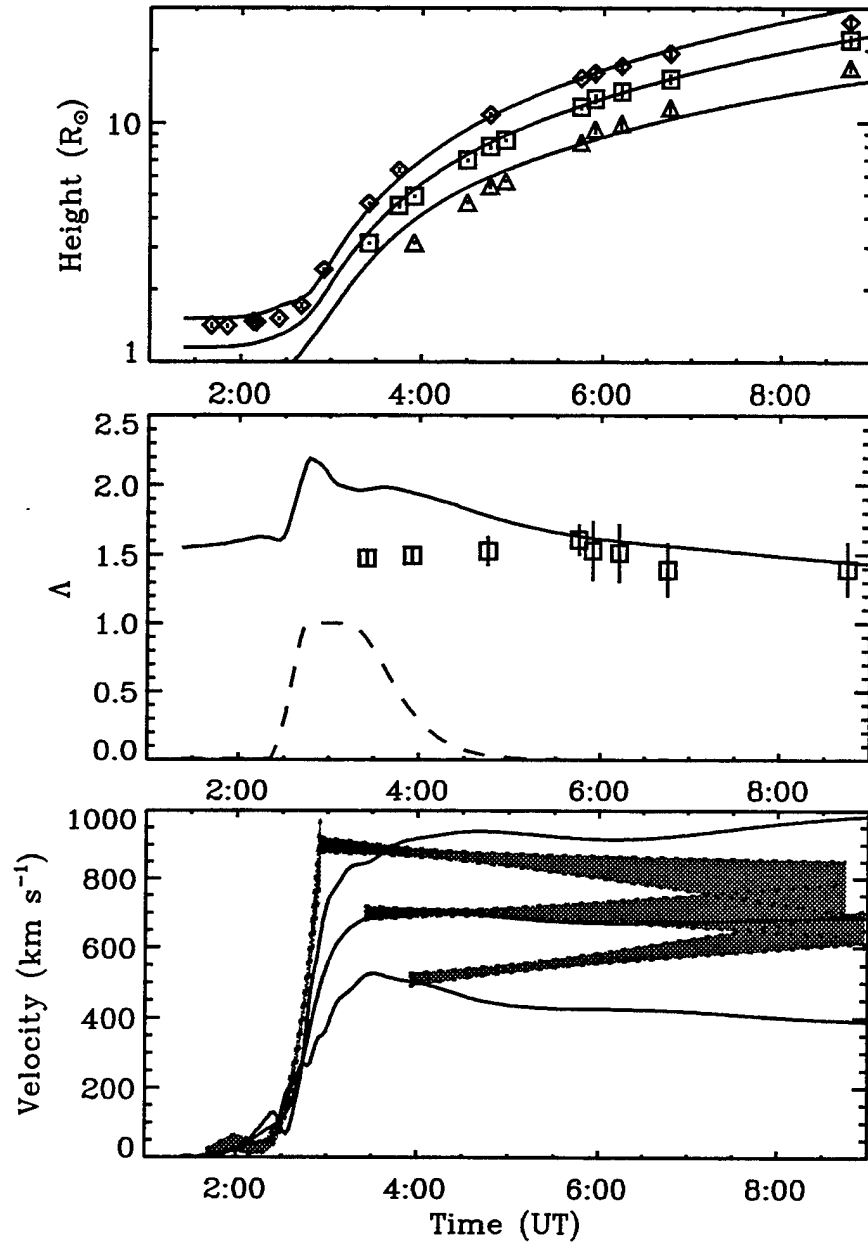


Fig. 6.— Same as Fig. 5, but for the February 23 CME. The height and velocity measurements are from Fig. 4.

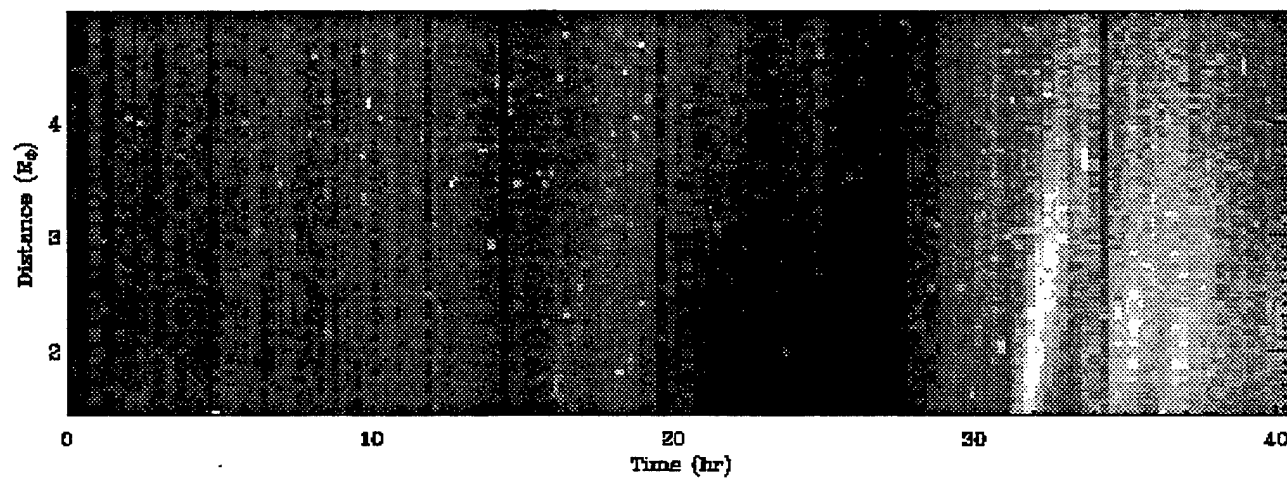


Fig. 7.— Intensity tracings of a sector in the north polar region plotted as a function of time, showing three polar jets at  $t = 32$ ,  $t = 35$ , and  $t = 37$  hrs.

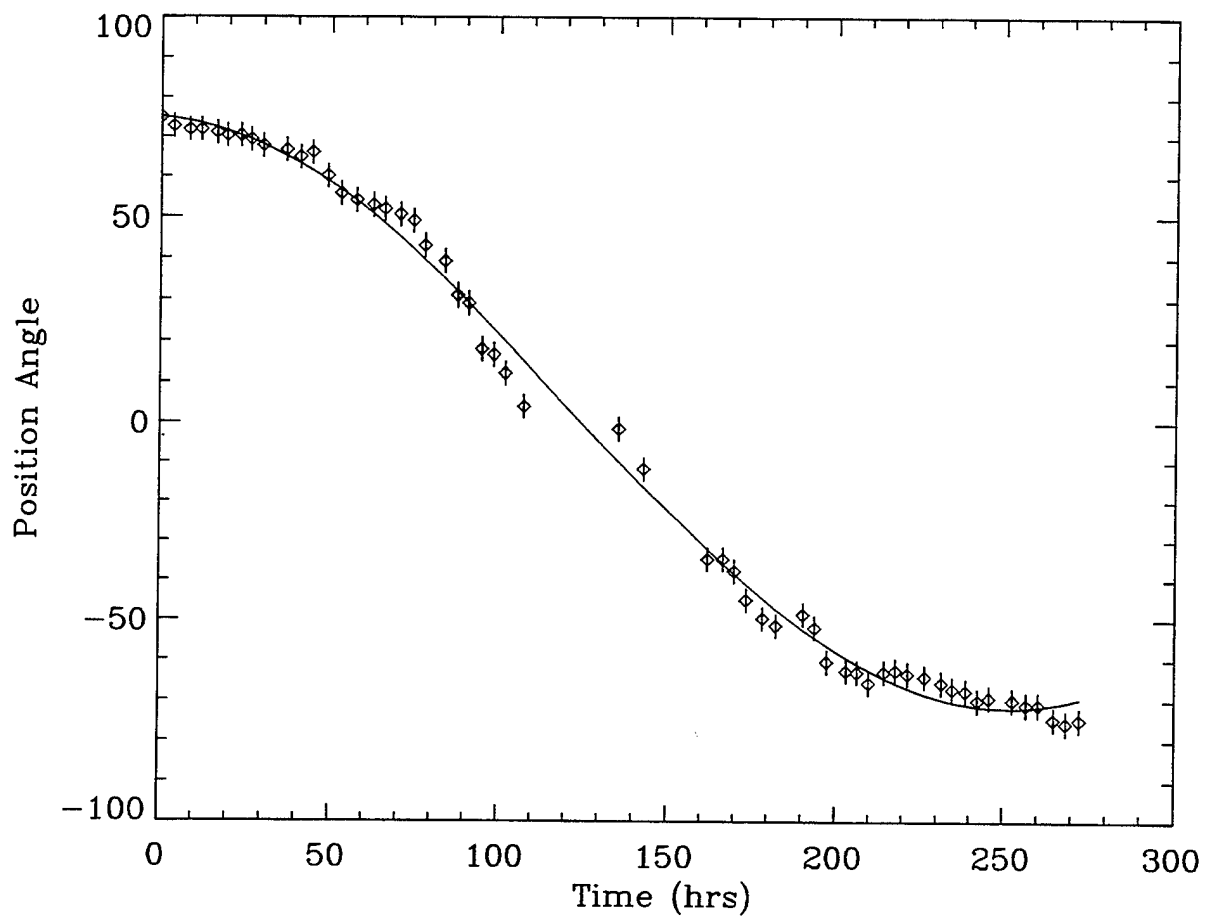


Fig. 8.— Position angle of a radial front of enhanced brightness observed in 1997 March, plotted as a function of time. A sine curve has been fitted to the data points.

REPORT DOCUMENTATION PAGE			Form Approved OMB No. 0704-0188	
Public reporting burden for this collection of information is estimated to average 1 hour per response, including the time for reviewing instructions, searching existing data sources, gathering and maintaining the data needed, and completing and reviewing the collection of information. Send comments regarding this burden estimate or any other aspect of this collection of information, including suggestions for reducing this burden, to Washington Headquarters Services, Directorate for Information Operations and Reports, 1215 Jefferson Davis Highway, Suite 1204, Arlington, VA 22202-4302, and to the Office of Management and Budget, Paperwork Reduction Project (0704-0188), Washington, DC 20503.				
1. AGENCY USE ONLY (Leave blank)		2. REPORT DATE SEPT 8, 1998		3. REPORT TYPE AND DATES COVERED ANNUAL 2/1/97 thru 1/31/98
4. TITLE AND SUBTITLE  Enhancement of LASCO C1, C2, and C3 Coronagraph Images			5. FUNDING NUMBERS  N00014-97-1-G023	
6. AUTHOR(S)  Margarita Karovska and Brian Wood				
7. PERFORMING ORGANIZATION NAME(S) AND ADDRESS(ES)  Smithsonian Astrophysical Observatory			8. PERFORMING ORGANIZATION REPORT NUMBER	
9. SPONSORING / MONITORING AGENCY NAME(S) AND ADDRESS(ES)			10. SPONSORING / MONITORING AGENCY REPORT NUMBER	
11. SUPPLEMENTARY NOTES				
12a. DISTRIBUTION / AVAILABILITY STATEMENT			12b. DISTRIBUTION CODE	
13. ABSTRACT (Maximum 200 words)  <p>The Large Angle Spectrometric Coronagraph (LASCO) onboard SOHO provides unprecedented views of the solar corona since January 1996. During the past year we carried out a study of the morphology and dynamical evolution of various structures in the solar corona including coronal mass ejections, and polar jets. We highlight in this report two examples of our analysis of CMEs (from 1997 April 30 and 1997 February 23), and the results of our testing of the viability of an MHD model of expanding flux rope developed by Chen et al. (1997). We also highlight results from our ongoing study of the dynamical evolution of structures in the solar polar regions. Our study was focused on a series of three compact jets of material ejected on 1997 March 22 from a point near the north pole. The results show evidence for substantial deceleration. The estimated initial ejection velocity is slightly below the Sun's escape velocity of <math>619 \text{ km s}^{-1}</math>. We conclude that the dynamical evolution of these jets is different from that of coronal mass ejections, which generally show continuous acceleration below <math>3-4 R_{\odot}</math>.</p>				
14. SUBJECT TERMS			15. NUMBER OF PAGES 12	
			16. PRICE CODE	
17. SECURITY CLASSIFICATION OF REPORT	18. SECURITY CLASSIFICATION OF THIS PAGE	19. SECURITY CLASSIFICATION OF ABSTRACT	20. LIMITATION OF ABSTRACT	